Published online 24 October 2017 *Nucleic Acids Research, 2017, Vol. 45, No. 22* ***12987–13003***
doi: 10.1093/nar/gkx979

Conserved structures formed by heterogeneous RNA sequences drive silencing of an inflammation responsive post-transcriptional operon

Abhijit Basu[1], Niyati Jain[2], Blanton S. Tolbert[2], Anton A. Komar[1] and Barsanjit Mazumder[1,*]

[1]Center for Gene Regulation in Health & Disease, Department of Biology, Geology and Environmental Sciences, Cleveland State University, 2121 Euclid Avenue, Cleveland, OH 44115, USA and [2]Department of Chemistry, Case Western Reserve University, Cleveland, OH 44106, USA

Received March 23, 2017; Revised October 06, 2017; Editorial Decision October 06, 2017; Accepted October 09, 2017

ABSTRACT

RNA–protein interactions with physiological outcomes usually rely on conserved sequences within the RNA element. By contrast, activity of the diverse gamma-interferon-activated inhibitor of translation (GAIT)-elements relies on the conserved RNA folding motifs rather than the conserved sequence motifs. These elements drive the translational silencing of a group of chemokine (CC/CXC) and chemokine receptor (CCR) mRNAs, thereby helping to resolve physiological inflammation. Despite sequence dissimilarity, these RNA elements adopt common secondary structures (as revealed by 2D-^{1}H NMR spectroscopy), providing a basis for their interaction with the RNA-binding GAIT complex. However, many of these elements (e.g. those derived from CCL22, CXCL13, CCR4 and ceruloplasmin (Cp) mRNAs) have substantially different affinities for GAIT complex binding. Toeprinting analysis shows that different positions within the overall conserved GAIT element structure contribute to differential affinities of the GAIT protein complex towards the elements. Thus, heterogeneity of GAIT elements may provide hierarchical fine-tuning of the resolution of inflammation.

INTRODUCTION

Post-transcriptional regulation of the expression of inflammatory molecules is emerging as an important strategy used by cells of myeloid origin to control inflammation and innate immunity (1–5). This involves a novel mechanism of translational silencing mediated by binding of a cytosolic protein complex to specific elements within the 3′ UTRs of target mRNAs. We first identified this mechanism in a model of IFN-γ induced synthesis of ceruloplasmin (Cp) in human monocytes (6–8). These studies showed that IFN-γ treatment induces phosphorylation of ribosomal protein L13a and its release from the 60S ribosomal subunit (8). The released phosphorylated L13a protein joins with glutamyl-prolyl-tRNA synthetase (EPRS), NS1-associated protein-1 (NSAP1), and glyceraldehyde 3-phosphate dehydrogenase (GAPDH) to form an RNA binding complex called IFN-gamma-activated-inhibitor of translation (GAIT) (9). The GAIT complex specifically binds to a 29-nt long GAIT element in the Cp 3′-untranslated region (UTR) (10) and blocks translation initiation. GAIT complex-dependent inhibition of translation initiation relies on interaction between the 3′UTR-bound GAIT complex and eIF4F-bound eIF4G, which prevents recruitment of the 43S pre-initiation complex (11). In human monocytes, translational silencing of Cp is only observed after the 16 h of IFN-γ treatment required to induce release of L13a from the 60S ribosomal subunit and formation of the active GAIT complex (8).

We subsequently demonstrated through a genome-wide screen that GAIT-mediated silencing is not unique to Cp, but rather controls translation of a number of mRNAs including several encoding chemokines and chemokine receptors (e.g. CCL22, CXCL13, CCR4, CCL8, CCL21, CCR3 and CCR6). This led us to hypothesize that coordinated control of mRNAs encoding proinflammatory proteins via the GAIT mediated mechanism might be an important cellular strategy to restrain inflammation and that the target mRNAs might represent an inflammation-responsive 'post-transcriptional operon' (12).

Support for this hypothesis and its physiological significance was provided by studies in macrophage-specific L13a knockout (KO) mice (13). Three human diseases, endotoxemia, atherosclerosis and colitis, were experimentally induced in this KO animal model by lipopolysaccharide (LPS) (13), high-fat diet (14) and dextran sodium sulfate (DSS) treatments (15), respectively. In all three cases, disease pathology was more severe in the KO animals than in controls. Upon induction of endotoxemia, L13a KO animals displayed more severe symptoms of inflammation than controls and more widespread infiltration of macrophages into major organs, resulting in greater tissue injury and re-

*To whom correspondence should be addressed. Tel: +1 216 687 2435; Fax: +1 216 687 6972; Email: b.mazumder@csuohio.edu

duced survival (13). The increased severity of atherosclerosis (14) and colitis (15) in L13a KO mice was evidenced by increased macrophage infiltration in the aortic plaque and intestinal epithelium, respectively. *Ex vivo* analysis of macrophages harvested from control mice after disease induction showed translational silencing of several GAIT complex target mRNAs, including those encoding CCL22, CXCL13, CCR3, CCR4, CCL3 and CCL11. In contrast, these mRNAs were not silenced in the KO mice, resulting in significantly higher steady state levels of the encoded chemokines and chemokine receptors (13). Persistent high-level expression of such pro-inflammatory molecules has been shown to contribute to the pathology of these and other diseases. Thus, GAIT-mediated translational silencing represents an important physiological self-defense mechanism.

The regulatory function of GAIT RNA elements has been postulated to depend on their ability to fold into specific stem–loop structures that are recognized and bound by the GAIT protein complex (6–10). It has been found, however, that regulatory RNA elements can accommodate extensive sequence variation (16). The canonical Cp GAIT element consists of 29 nucleotides that form a 6-bp helical stem, an asymmetric internal bulge, a weak 3-bp distal helix and a 5-nt loop (10). Mutations that preserve or disrupt this structure have corresponding effects on Cp translational silencing. It has been predicted that other GAIT elements can potentially form similar stem–loop structures while accommodating the diversity of nucleotide lengths and sequences (12,13). However, it has not been known whether these potential GAIT elements in the newly identified chemokine and chemokine receptor mRNAs can indeed adopt the predicted structures and whether sequence variations of these elements could alter their relative affinity for the RNA-binding GAIT protein complex.

In this study, we have used a combination of approaches, including RNA-electrophoretic mobility shift assay (EMSA), *in vitro* translational silencing assay, toeprinting and 2D and 1D NMR spectroscopy to dissect the structure and function of several newly identified GAIT elements. We have found that while all these elements can adopt similar stem loop structures (as revealed by 2D-^{1}H and 1D-^{1}H NMR spectroscopy), they, at the same time, show differential affinities toward GAIT protein complex. Toeprinting analyses revealed that different positions within the overall conserved GAIT element structure contribute to these differences in binding affinity. Heterogeneity in GAIT binding affinities might create a silencing hierarchy among GAIT target mRNAs that is important for fine-tuning the resolution of inflammation. Together, these results establish a new paradigm for translational control of gene expression by a family of sequence-unrelated but structurally conserved functional RNA elements that has broad physiological significance.

MATERIALS AND METHODS

In silico prediction of GAIT RNA element structures

3′ UTR sequences (500 nucleotides maximum) from candidate human and murine mRNAs were locally aligned pairwise with the human Cp GAIT element using the FOLDALIGN program (foldalign.ku.dk/server/index.html), which simultaneously folds and aligns two or more RNA sequences and can make structure predictions (17–19). The resulting hits were then folded using the 'RNAstructure' web server (http://rna.urmc.rochester.edu/RNAstructure.html).

Preparation of GAIT RNA elements for NMR analysis

The RNAs (Cp, CXCL13, CCL22 and CCR4) were purchased as untreated crude synthetic oligonucleotides from GE Dharmacon. The RNAs were purified by 12–16% denaturing PAGE, excised from gels and electroeluted. Prior to PAGE purification the samples were deprotected as specified by Dharmacon (http://dharmacon.gelifesciences.com/uploadedFiles/Resources/deprotection-of-2-ace-protected-rnai-protocol.pdf). The samples were further purified by HPLC. Anion exchange was performed using a DNAPac PA 200 9 × 250 mm column (buffer A: 20 mM Tris pH 8, and buffer B: 20 mM Tris and 2 M NaOH pH 8 made in RNase-free water). The samples were desalted using Millipore Amicon® Ultra-4 centrifugal filter devices. The samples were annealed by heating at 95°C for 3 min followed by snap cooling on ice. Native polyacrylamide gel was run to check the conformational homogeneity. All the RNA migrated as single species except CCL22 that folded into two species; the faster running predominant species (95%) migrated closer to the other GAIT elements and was analyzed by NMR. The samples were dried by using a SpeedVac (Eppendorf Vacufuge plus), resuspended into 10 mM K_2HPO_4, 10 mM KCl (pH 6.0) and 90% H_2O, 10% D_2O for NMR analysis. All NMR experiments were carried out using RNA concentrations that ranged from 0.5 to 0.8 mM. The concentrations were determined using theoretical molar extinction coefficients that were calculated using Nanodrop 2000 calculation tool.

NMR data acquisition, processing and analysis

Two-dimensional NMR experiments were carried out using Bruker Avance (800-MHz) high field NMR spectrometer equipped with cryogenically cooled, HCN triple resonance probes and a *z*-axis pulsed field gradient accessory. To check RNA conformational homogeneity and purity, 1D-^{1}H NMR experiments were performed. All NMR data were processed by NMRPipe/NMRDraw (20) and analyzed using the software NMRView J (21). Exchangeable ^{1}H spectra were measured at 288 K with the Watergate NOESY (τ_m = 150 ms) pulse sequence.

Preparation of cytosolic extracts from U937 cells

Human monocytic U937 cells (American Type Culture Collection, Rockville, MD; CRL 1593.2) were cultured in RPMI 1640 medium with 10% heat-inactivated fetal bovine serum, 2 mM glutamine, and 100 U/ml penicillin and streptomycin at 37°C and 5% CO_2. To induce GAIT complex-mediated translational silencing, exponentially growing U937 cells were treated with 500 U/ml human IFN-γ (R&D Systems) for up to 24 h. Cells were then

collected by centrifugation, washed with ice-cold PBS and resuspended in lysis buffer [50 mM Tris (pH 7.6), 50 mM NaCl, 1 mM phenylmethylsulfonyl fluoride (PMSF), and 1 mM dithiothreitol (DTT)]. Cell suspensions were subjected to three freeze-thaw cycles, passed several times through a 26-gauge needle, and then centrifuged at 10 000 × g for 30 min. Supernatants were collected and used in RNA EMSA.

Animal handling and preparation of mouse peritoneal macrophage extracts

All experiments involving mice were carried out in accordance with National Institutes of Health and Institutional Animal Care and Use Committee guidelines. Saline or bacterial lipopolysaccharide (LPS, Sigma-Aldrich) was injected intraperitoneally in age- and sex-matched control ($L13a^{flox/flox}$) or L13a KO ($L13a^{flox/flox}$ LysM $Cre^{+/+}$) mice (13). After 48 h of injection, mice were euthanized and macrophages were collected by peritoneal lavage with ice-cold PBS. Protein extracts were prepared from mouse macrophages as described above for U937 cells.

Immunodepletion of L13a from cellular lysate

L13a protein was immunodepleted from U937 and mouse macrophage extracts by incubating the extracts with an anti-L13a antibody raised against a peptide NVEKKIDKYTEVLKTHG near the C terminus of human L13a (8). This antibody specifically recognizes both human and mouse L13a.

3′ biotinylation of RNAs

Synthetic custom RNAs were purchased from Integrated DNA Technologies (IDT). 3′ ends of the RNAs were biotinylated using the Pierce RNA 3′ end biotinylation kit (Thermo Scientific, Catalog # 20160) following the manufacturer's protocol.

RNA EMSA

For RNA EMSA experiments, 3′-biotinylated RNAs (15 fmol) were incubated for 30 min on ice with cellular extracts in a 20 μl reaction mixture containing 10 mM HEPES (pH 7.3), 20 mM KCl, 1 mM $MgCl_2$, 1 mM DTT, 5% glycerol, 10 μg yeast tRNA and 40 U RNasin (Promega). For competition experiments, 3′-labeled and unlabeled competitor RNAs were added to the extract. RNA–protein complexes were separated by native gel electrophoresis (5% polyacrylamide in 0.5× Tris-borate EDTA [TBE] buffer) at 4°C, transferred to a nylon membrane and detected by chemiluminescence using the Pierce Lightshift chemiluminescent RNA EMSA kit (Thermo Scientific, Catalog # 20158).

Determination of GAIT element–mediated translational silencing activity in a cell-free *in* vitro translation system

GAIT elements were cloned downstream of a luciferase reporter gene under T7 promoter control such that the elements will be present in the luciferase 3′UTR. cRNAs of the hybrid reporter luciferase-GAIT element genes were generated by *in vitro* transcription. The cRNAs (100 ng) were subjected to *in vitro* translation using rabbit reticulocyte lysates (Promega) in the presence of [^{35}S]-methionine. 4 μg of U937 cell or macrophage extracts were used to test the translational silencing activity. A 10 μl aliquot of the translation reaction mixture was resolved by SDS-PAGE (10% polyacrylamide) and labeled proteins were visualized by autoradiography. For quantification the ratio of the band intensities of the luciferase protein and T7 gene10 protein (as internal control) were determined using NIH image J64 software. The percent inhibition was determined by comparing with the control lane with no extract.

Determination of equilibrium dissociation constants for GAIT RNA–protein complexes

Quantitative analysis of interactions between GAIT RNA elements and the GAIT protein complex was done by EMSA essentially as described by Ryder *et al.* (22). Since the active concentration of GAIT protein complex in the cellular extracts used in the experiments was not known, we arbitrarily assigned it to be 1/100 of the total extract concentration used. We assumed that the stoichiometry of binding is 1:1. Direct titration reactions were plotted as fraction of bound RNA versus GAIT/extract concentration. Competition reactions were plotted as the fraction of bound labeled RNA versus the concentration of unlabeled competitor. The data were fit using non-linear least squares methods with either a standard Hill equation and/or a modified Hill equation that can compensate for deviations from ideal conditions (e.g. incomplete RNA binding, cooperative binding, etc.) (22). 15 fmol of 5′-end-labeled probes were used in the reactions. In competition experiments 1×, 2×, 5×, 10×, 20×, 50× and 100× excesses of unlabeled probes were used, respectively. All experiments were performed in triplicate and standard deviations were included in the plot.

Toe printing assays

RNA segments (110 nucleotides long) containing GAIT elements and flanking sequences from the 3′ UTRs of human Cp, CCL22, CXCL13 and CCR4 mRNAs were transcribed *in vitro* with T7 RNA polymerase from PCR-generated DNA templates using mMESSAGEmMACHINE kit (Ambion, Catalog # 1344). Toeprinting assays were performed as previously described (23) with minor modifications. 200 ng of *in vitro* synthesized RNAs were annealed to RNA-specific primers (5′ end-labeled with [γ-^{32}P]ATP (3000 Ci/mmole) using T4 polynucleotide kinase) in 50 mM Tris (pH 7.5) and 0.1 mM EDTA by incubating at 90°C for 2 min followed by slow cooling to room temperature. After primer annealing, the RNAs were incubated with cytosolic extracts prepared from IFN-γ-treated U937 cells or untreated cells using the binding conditions described for RNA EMSA. The position of GAIT protein complexes bound to the RNAs was determined by primer extension/reverse transcription using five units of Avian Myeloblastosis Virus (AMV) reverse transcriptase (Promega) and 400 μM each dTTP, dGTP, dCTP and dATP. After incubation at 37°C for 1 h, the samples were

sequentially extracted with phenol/chloroform and chloroform alone and then ethanol-precipitated. The cDNAs produced in the reactions were separated under denaturing conditions on 8% polyacrylamide/7 M urea gels, which were subsequently dried and subjected to autoradiography. Dideoxy-sequencing reactions were conducted on the same RNAs using the same primers as used for primer extension and were loaded on the same gel alongside the cDNAs generated in the primer extension reaction.

RESULTS

Sequence-unrelated human and mouse CCL22, CCR4 and CXCL13 GAIT-elements are predicted to fold into stem–loop structures similar to that of the canonical Cp GAIT element

Using *ex vivo* (cellular) (12) and *in vivo* (murine) (13–15) models we have previously identified a cohort of chemokine and chemokine receptor mRNAs that are regulated by an L13a-dependent translational silencing mechanism. Since they are regulated in this way these mRNAs are expected to harbor active GAIT elements in their 3′UTRs; however, no sequence homology was found between the canonical GAIT element in the human Cp mRNA (10) and the newly identified target mRNAs. Therefore, we hypothesized that those structural aspects of the mRNAs rather than sequence features might direct GAIT-mediated control of their translation. To identify potential folding homologies, the 3′UTRs of the (human and mouse) target mRNA sequences were tested for folding homology against the human Cp GAIT element (10) using 'Foldalign' (http://foldalign.ku.dk) (17–19) and 'RNAstructure' (http://rna.urmc.rochester.edu/RNAstructure.html) programs. Pairwise structural RNA alignments and mutual motif searches identified a number of predicted stem–loop structures in all target mRNAs that were similar to the structure formed by the human Cp GAIT element (Figure 1). These segments were tested for their ability to bind GAIT protein complex and support inhibition of translation (see below). Only the validated elements are presented in Figure 1. Interestingly, the stem–loop structures predicted for the newly identified CCL22, CCR4 and CXCL13 GAIT elements showed substantial differences (up to 10-fold) in thermodynamic stability (as reflected by predicted ΔG values) when compared to the canonical Cp GAIT element. The stem–loop of the human Cp GAIT element was least stable (ΔG = –1.2 kcal/mol), followed by human CCR4 (ΔG = –1.7 kcal/mol), mouse CCL22 (ΔG = –3.4 kcal/mol), human CXCL13 (ΔG = –3.6 kcal/mol), mouse CCR4 (ΔG = –5.1 kcal/mol), human CCL22 (ΔG = –10.5 kcal/mol) and mouse CXCL13 (ΔG = –12 kcal/mol).

NMR analyses confirm that the *in silico* predicted structures of the heterogeneous GAIT elements are formed in solution

To confirm the *in silico* folding predictions, the secondary structure of each GAIT element was verified using 2D NMR spectroscopy wherein the imino protons show diagnostic chemical shifts for canonical and non-canonical base pairs. ^{1}H–^{1}H NOESY spectra for GAIT RNA elements derived from human Cp, CCL22, CCR4 and CXCL13 mRNAs were collected in water (288K). Imino protons for canonical A·U base pairs resonate in the region between 13–15 ppm, whereas imino protons for canonical G·C and G·U base pairs typically resonate between 12 and 13.5 ppm and 10 and 12 ppm, respectively. The observed chemical shifts, well resolved with mainly imino resonances between 10 and 13.5 ppm (which are typical of canonical Watson–Crick or G.U wobble base pairing), indicate that all of the GAIT elements adopt structures that are consistent with *in silico* predictions, despite their differences in primary sequence.

In agreement with the predicted structure (Figure 1), the ^{1}H–^{1}H NOESY spectra of Cp (Figure 2A) shows the imino chemical shifts and the sequential NOE cross peaks for consecutive G·C and A·U base pairs in the lower helix. Assignment of the imino proton resonances proves the formation of the predicted base pairs in the lower stem. For CCL22 the three consecutive G·C base pair walking to A·U base pair in the lower helix is evident from the spectra (Figure 2B). A peak resonating at ∼11.3 ppm was assigned to U5 though the NOE cross peaks for the closing G·U wobble base pair were not observe due to rapid solvent exchange. The chemical shift for A19·U11 base pair walking to consecutive G12·C18 base pair in the upper helix was detected. The spectra of CCR4 (Figure 2C) show signature NOE cross peaks and chemical shifts for G·U wobble (G2·U24) base pair. The sequential imino proton walk between G·C base pairs and G·U wobble base pair are observed in the lower helix. Additionally the spectra show the imino resonances for two G·C base pairs providing clear evidence for formation of upper helix. Due to rapid solvent exchange during the mixing time the imino shifts for the A·U base pairs were not observed; however, 1D-^{1}H NMR confirmed the WC base pairs from the upper helix (Supplementary Figure S1). Like CCR4, the spectra of CXCL13 (Figure 2D) show upfield-shifted resonances and strong cross-peaks between G2 and U27 residues indicating the formation of wobble G·U base pair. The other G and U residues predicted to form a standard Watson–Crick G·C and A·U base pair in the lower helix yield observable imino resonances and sequential NOE cross-peaks in the region between ∼12 to ∼13.5 ppm. These imino resonances were assigned to G1, G3, G25 and U5. There was no strong evidence for base pairing in the upper helix beside G·C base pair between G11 and C19. Additional weak peaks were observed in the 1D NMR spectra that are non-canonical base pairs that are often found in loop regions (Supplementary Figure S1). Overall, the NMR data confirm that the analyzed GAIT elements adopt folds that are consistent with the *in silico* predictions.

Human and mouse CCL22, CCR4 and CXCL13 *in silico*-predicted GAIT elements can form L13a-dependent RNA-binding protein complexes

To assess functional activity of the *in silico*-predicted GAIT elements, corresponding RNA fragments derived from CCL22, CCR4 and CXCL13 mRNAs were 3′-biotinylated and tested for GAIT complex binding by electrophoretic mobility shift assay (EMSA) in comparison to the canonical Cp GAIT element. Characteristic gel shifts indicating formation of RNA–protein complexes were observed for all of the human mRNA derived GAIT-elements after their incu-

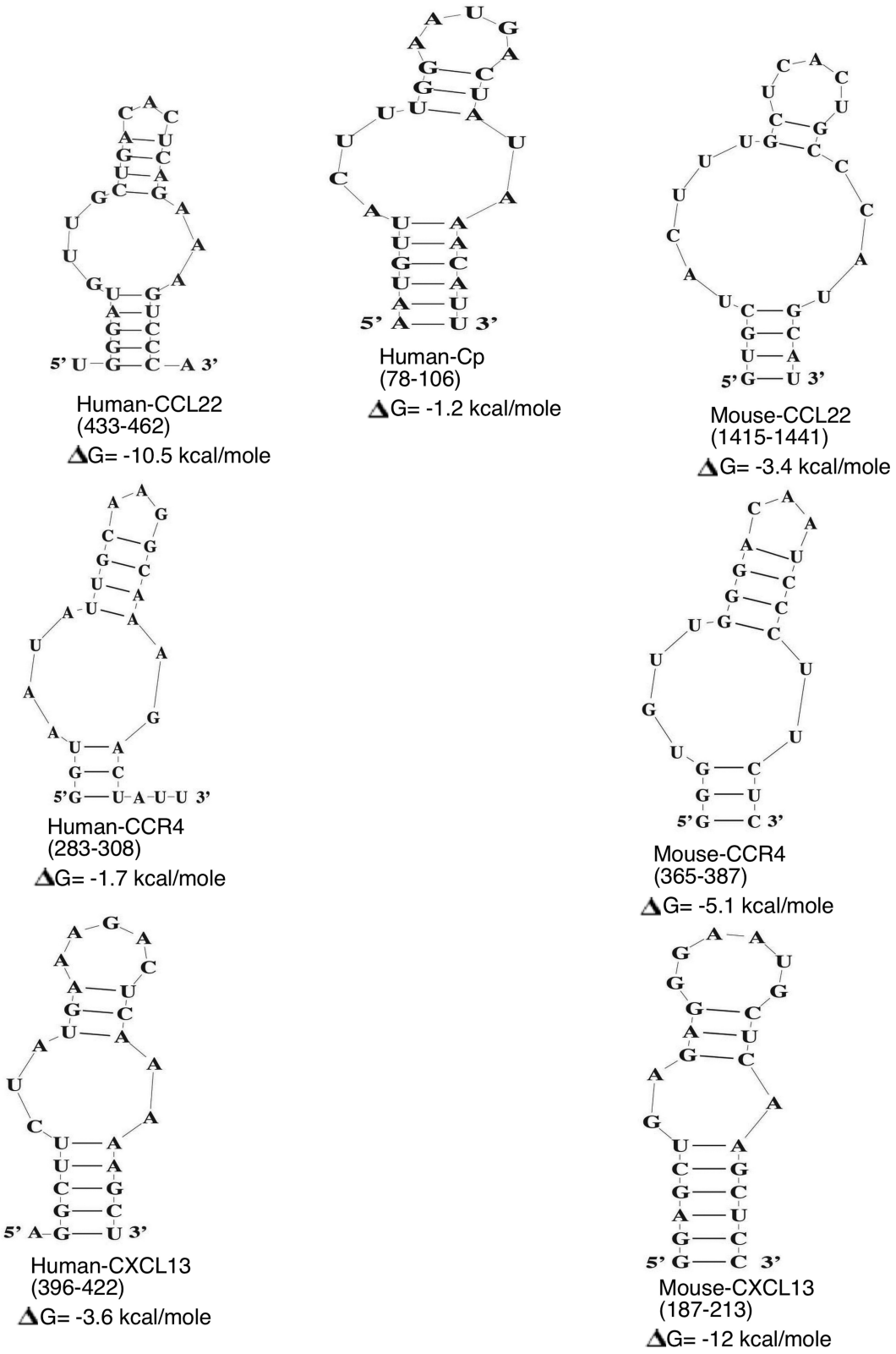

Figure 1. Sequence-unrelated human and mouse CCL22, CCR4 and CXCL13 GAIT-elements are predicted to fold into similar stem–loop structures. RNA structure and free energy predictions were made for the 3′UTRs of human and mouse CCL22, CCR4 and CXCL13 using 'FOLDALIGN' and 'RNAstructure' programs. From among the potential folding patterns identified for each RNA element, those with the lowest free energy and highest similarity to the canonical Cp GAIT element are shown. These sequence elements were subsequently subjected to NMR analysis and GAIT complex binding assays (see Figure 2, Supplementary Figure S1 and Figure 3). The numbers in parentheses indicate nucleotide (nt) number where 1 is the first nt after the stop codon.

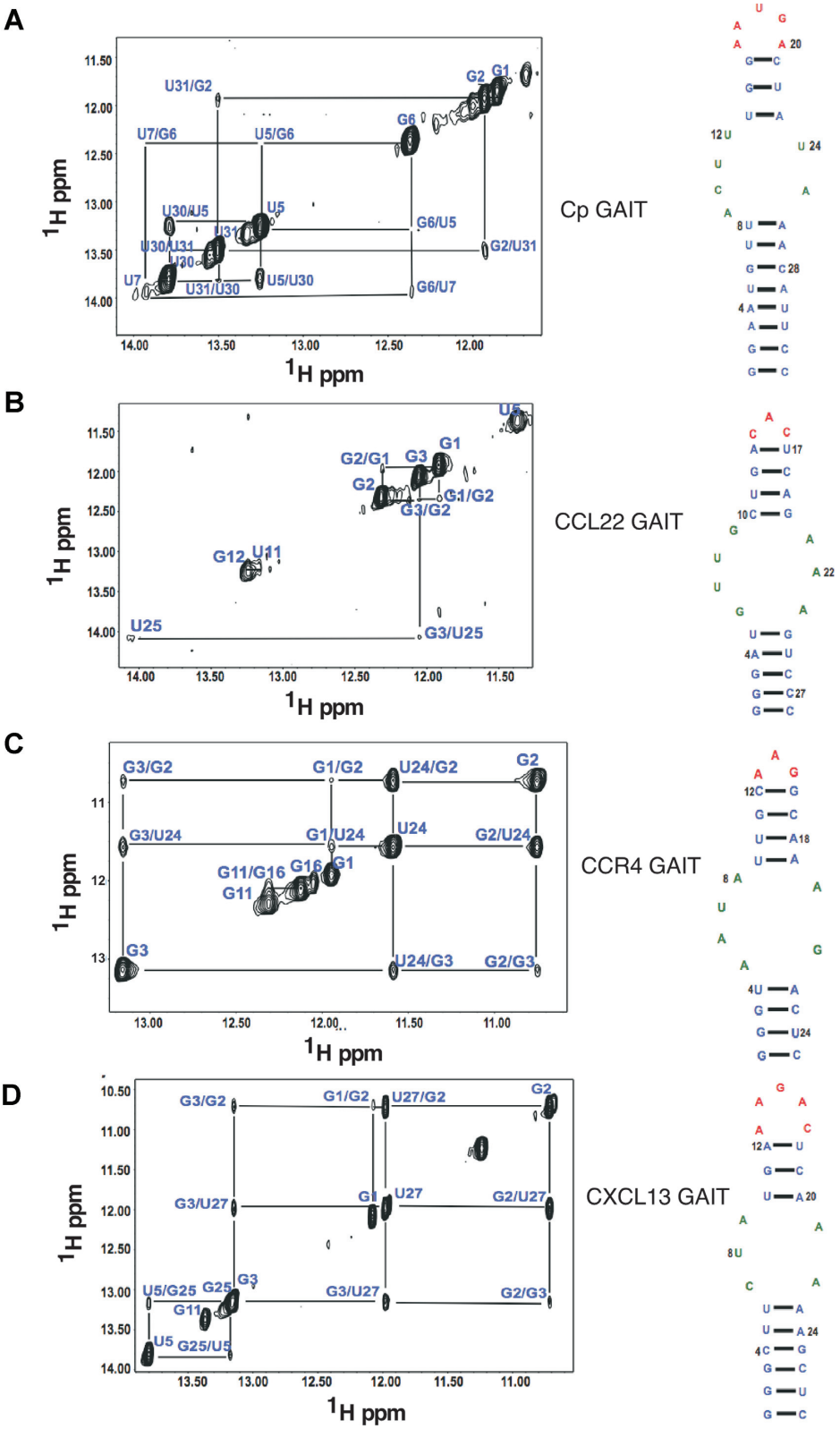

Figure 2. NMR spectroscopic analysis of Cp, CCL22, CXCL13 and CCR4 GAIT RNA elements confirms the *in silico*-predicted structures. ^{1}H–^{1}H NOESY spectra (800 MHz, $\tau_m = 150$ ms) of the GAIT elements of human Cp (**A**), CCL22 (**B**), CCR4 (**C**) and CXCL13 (**D**) showing NOE cross peaks and imino resonances between 10 and 14 ppm (typical for canonical Watson–Crick or G.U wobble base pairing). These results indicate that all of the analyzed GAIT elements adopt structures that are consistent with *in silico* predictions, despite differences in their primary sequences. ^{1}H–^{1}H NOESY spectra collected in 10 mM K_2HPO_4, 10 mM KCl (pH 6.0) and 90% H_2O and 10% D_2O at 288 K. The RNA secondary structure of each element is also shown on the right.

bation with cell extracts prepared from U937 human monocytic cells treated with IFN-γ for 24 h (but not 0 or 8 h) (Figure 3A). Pre-treatment of the extracts with anti-L13a antibody (but not control IgG) led to abrogation of RNA–protein complex formation (Figure 3A), demonstrating its strong dependence on L13a. Complex formation was also abrogated by self-competition with 10- and 50-fold molar excess of unlabeled RNA, thus showing specificity of the complex formation (Figure 3B).

To test RNA–protein complex formation for murine CCL22, CCR4 and CXCL13 GAIT elements, extracts were prepared from macrophages harvested from lipopolysaccharide (LPS)-treated mice. Our previous work showed that injection of LPS in mice induces L13a-dependent translation silencing activity (13). RNA EMSA analysis demonstrated formation of a specific RNA–protein complex when CCL22, CCR4 and CXCL13 GAIT elements were incubated with extracts from macrophages of LPS-treated, but not saline-treated, mice (Figure 3C). As observed for the human GAIT elements, formation of the murine complexes was blocked by self-competition with unlabeled RNA probe or immunodepletion of L13a from the extracts with anti-L13a antibody. L13a-dependence was also illustrated by the absence of complex formation with extracts prepared from macrophages harvested from LPS-treated L13a KO mice (Figure 3C). Together, these results demonstrate presence of an inducible GAIT element binding activity in human and mouse myeloid lineage cells that specifically recognizes GAIT elements in CCL22, CCR4 and CXCL13 mRNAs.

GAIT RNA element-GAIT protein complex binding is species-independent

There are several fundamental differences in innate immune and inflammatory responses between mice and humans (24). In addition, while the RNA-binding GAIT protein complex originally defined in human myeloid cells is heterotetrameric and consists of phospho-L13a, EPRS, NSAP1 and GAPDH (9) the corresponding complex in mice is heterotrimeric, lacking NSAP1 (25). To test whether this or other species-specific differences would impact GAIT complex binding to GAIT RNA elements, we performed RNA EMSA analyses using different combinations of human- and mouse-derived cell extracts and labeled GAIT RNA element probes. This showed that human-derived GAIT elements could form specific RNA-binding GAIT complexes with proteins in mouse cell extracts and vice versa (Figure 4A). The inter-species GAIT RNA–protein complexes comigrated on gels with complexes formed with RNA elements and extracts from the same species and were also specific (self-competed with unlabeled RNA) and L13a-dependent (Figure 4A and B). Thus, despite differences in the composition of the GAIT protein complex between mice and humans, complex formation is species-independent (at least within human and mouse).

The newly identified CCL22, CCR4 and CXCL13 GAIT elements support translational silencing

To directly test the ability of the newly identified CCL22, CCR4 and CXCL13 GAIT elements to drive translational silencing, we conducted *in vitro* translation silencing experiments. In these studies, reporter constructs in which GAIT elements derived from human and mouse CCL22, CCR4 and CXCL13 were inserted into the 3′UTR of the luciferase mRNA. These mRNAs were translated in a rabbit reticulocyte lysate (RRL) cell-free translation system, as previously described (6–8). Addition of extracts prepared from IFN-γ-treated human monocytic cells U937 to the system resulted in specific suppression of translation of not only human (Figure 5A), but also mouse (Figure 5B) chimeric GAIT element-containing luciferase mRNAs. As observed for GAIT element binding in RNA EMSA analyses (Figure 3), translational silencing was only conferred by extracts of U937 cells when the cells were treated with IFN-γ for 24 h (not untreated or 8 h IFN-γ treated) and was abrogated by immunodepletion of L13a from extracts (Figure 5A and B).

In vitro translation silencing experiments were also performed using extracts prepared from macrophages of LPS-treated mice as a source of GAIT protein complex. In our previous work, such extracts demonstrated translational silencing of RNAs containing the Cp GAIT element (13). Here, we found that macrophage extracts from LPS (but not saline)-treated mice can mediate translation silencing of RNAs containing either mouse (Figure 6A) or human (Figure 6b) CCL22, CCR4 and CXCL13 -derived GAIT elements. L13a-dependence of this activity was shown through use of extracts prepared from LPS-treated L13a-KO mice. Figures 5 and 6 the images are the representatives of triplicate. The quantitation of the translational silencing with standard deviations showed in the left panels of Figures 5A, B, 6A and B. The translational silencing activity of human and mouse myeloid cell extracts were verified (Supplementary Figure S2) using authentic GAIT element from Cp 3′UTR as a positive control based on our numerous previous studies (10–15). With both human and mouse extracts, translation of a RNA consisting of only reporter luciferase without the GAIT element (data not shown) and T7 gene10 RNA (used as an internal control with irrelevant sequence) was insensitive to translation inhibition, thus showing that the suppressed translation of chimeric luciferase-CCL22, -CCR4 and -CXCL13 reporter constructs is GAIT-element dependent. Together, these experiments demonstrate that the *in silico* identified GAIT elements in CCL22, CCR4 and CXCL13 mRNAs can indeed direct translational silencing by L13a-dependent GAIT complex and that this activity is species-independent, at least between mouse and human.

CCL22, CCR4 and CXCL13 -derived GAIT elements bind GAIT protein complex with different affinities

GAIT complex interaction with the human Cp GAIT element appears to be quite stable since binding is observed by EMSA using complex mixtures of proteins such as cell extracts (6,8). We found that this is also the case for the newly identified CCL22, CCR4 and CXCL13 GAIT elements (Figures 3 and 4). However, it was not clear whether at closer resolution there might be differences in the affinity of different GAIT elements toward the GAIT protein complex. Neither the exact mechanism of GAIT RNA–protein complex assembly nor the determinants of RNA–protein binding affinity are currently known. It is believed

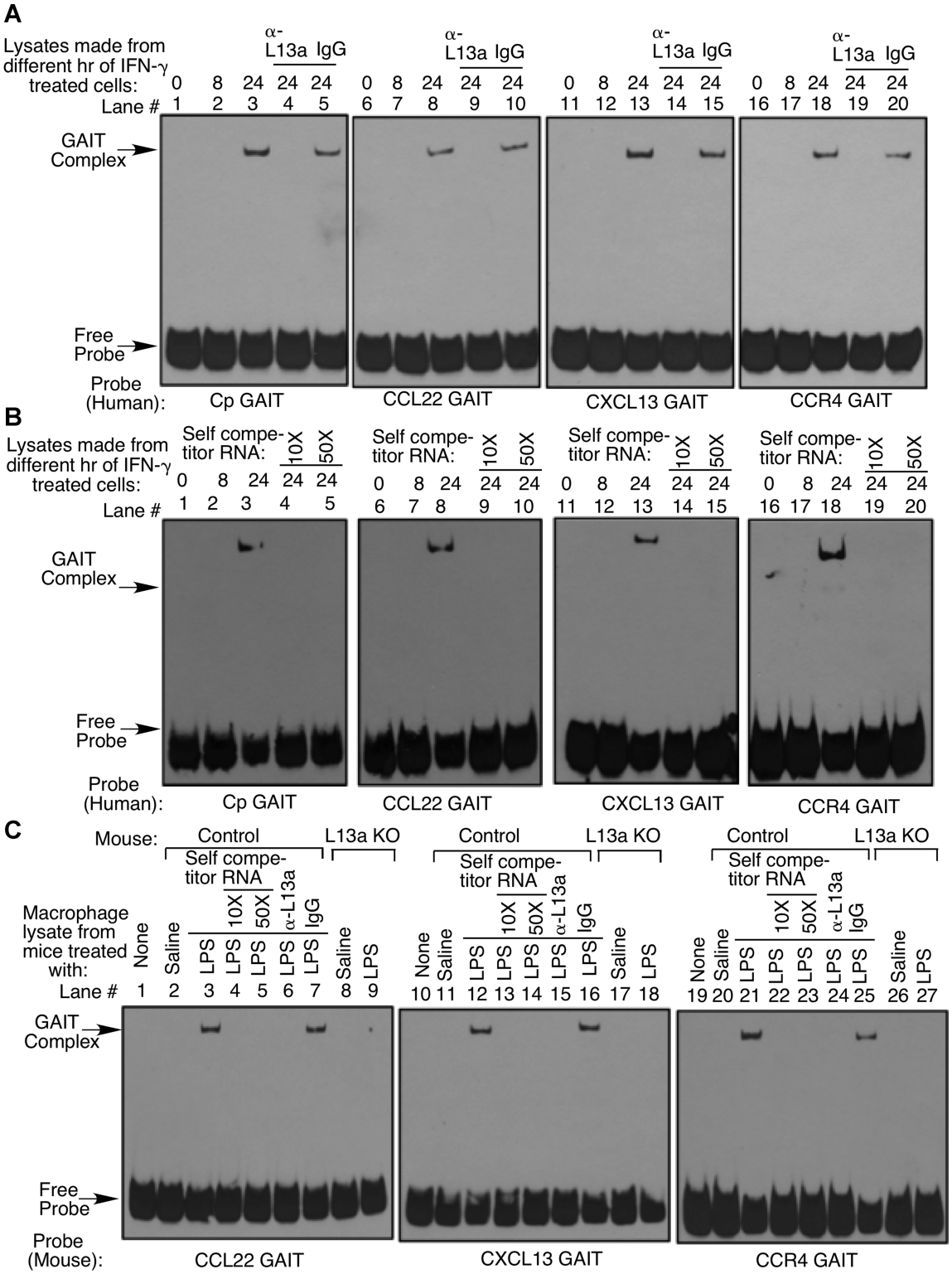

Figure 3. The *in silico*-identified GAIT elements in human and murine chemokine mRNAs form L13a-dependent, specific RNA-binding complexes. (**A**) RNA EMSA analysis shows formation of complexes between human CCL22, CCR4 and CXCL13 GAIT elements and interferon-inducible proteins in human U937 cells that are L13a-dependent and comigrate with canonical Cp GAIT element complexes. Binding reactions were performed with biotin labeled GAIT element probes and extracts from U937 cells that were untreated or treated with IFN-γ for 8 or 24 h. To show L13a-dependence, extract made from 24 h of IFN-γ treated cells was preincubated with anti-L13a or IgG control antibodies. (**B**) Self-competition with unlabeled GAIT RNA elements (10- and 50-fold molar excess) eliminates GAIT RNA–protein complex formation. EMSA was performed as in (A). (**C**) RNA EMSA analysis shows L13a-dependent binding of murine GAIT-elements by proteins in macrophage extracts prepared from LPS-treated mice. EMSA (including self-competition with unlabeled GAIT element probes and L13a immunodepletion) was performed as in (A) using extracts prepared from macrophages of control (L13a wild type) or L13aKO mice that were treated with saline or LPS. (A–C) Shifted complexes and unreacted probes are indicated with arrows.

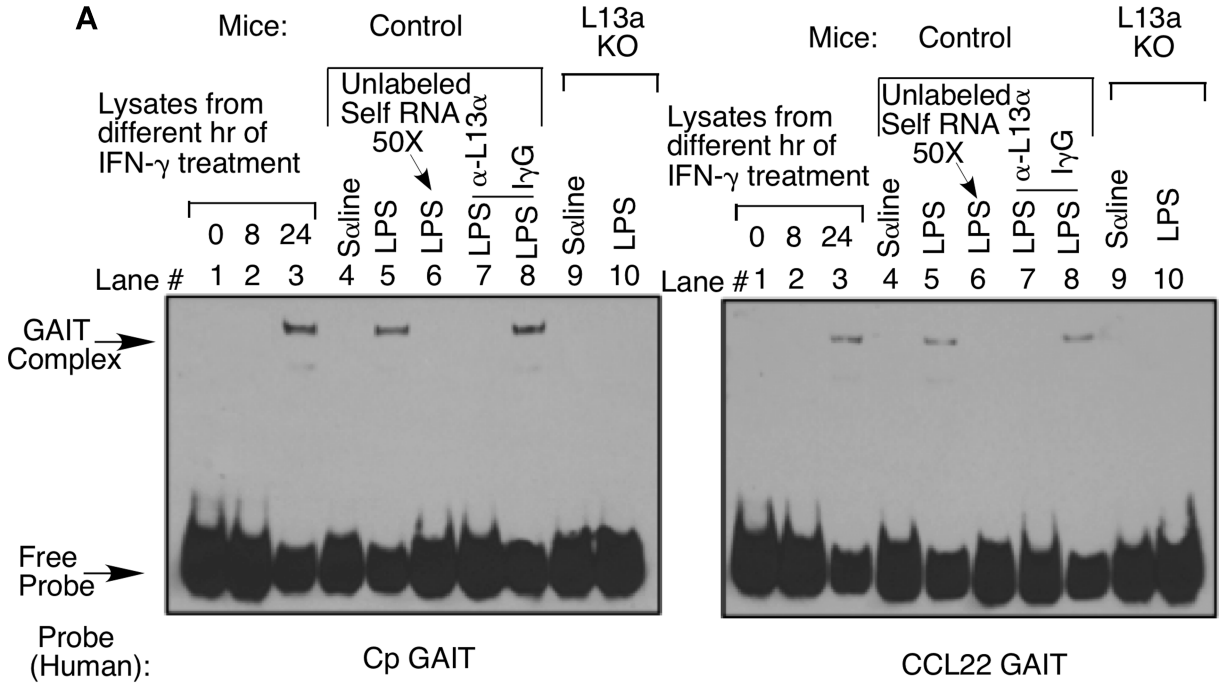

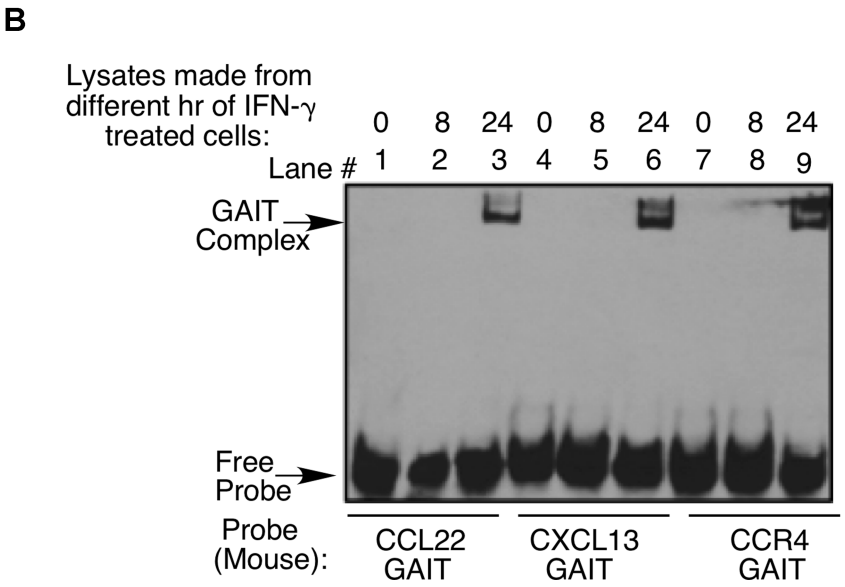

Figure 4. GAIT RNA element-GAIT protein complex binding is species-independent. (**A**) RNA EMSA analysis shows that GAIT elements from human Cp and CCL22 mRNAs support RNA-binding complex formation when incubated with cytosolic extracts prepared from IFN-γ-treated human U937 cells or from peritoneal macrophages of LPS-treated mice. L13a-immunodepletion and self-competition with unlabeled GAIT RNA element probes (10- and 50-fold molar excess) eliminates binding. (**B**) RNA EMSA analysis shows that GAIT elements from mouse CCL22, CXCL13 and CCR4 mRNAs support RNA-binding complex formation when incubated with cytosolic extract prepared from IFN-γ-treated U937 cells. All extracts were prepared as in Figure 3. Shifted complexes and unreacted probes are indicated with arrows.

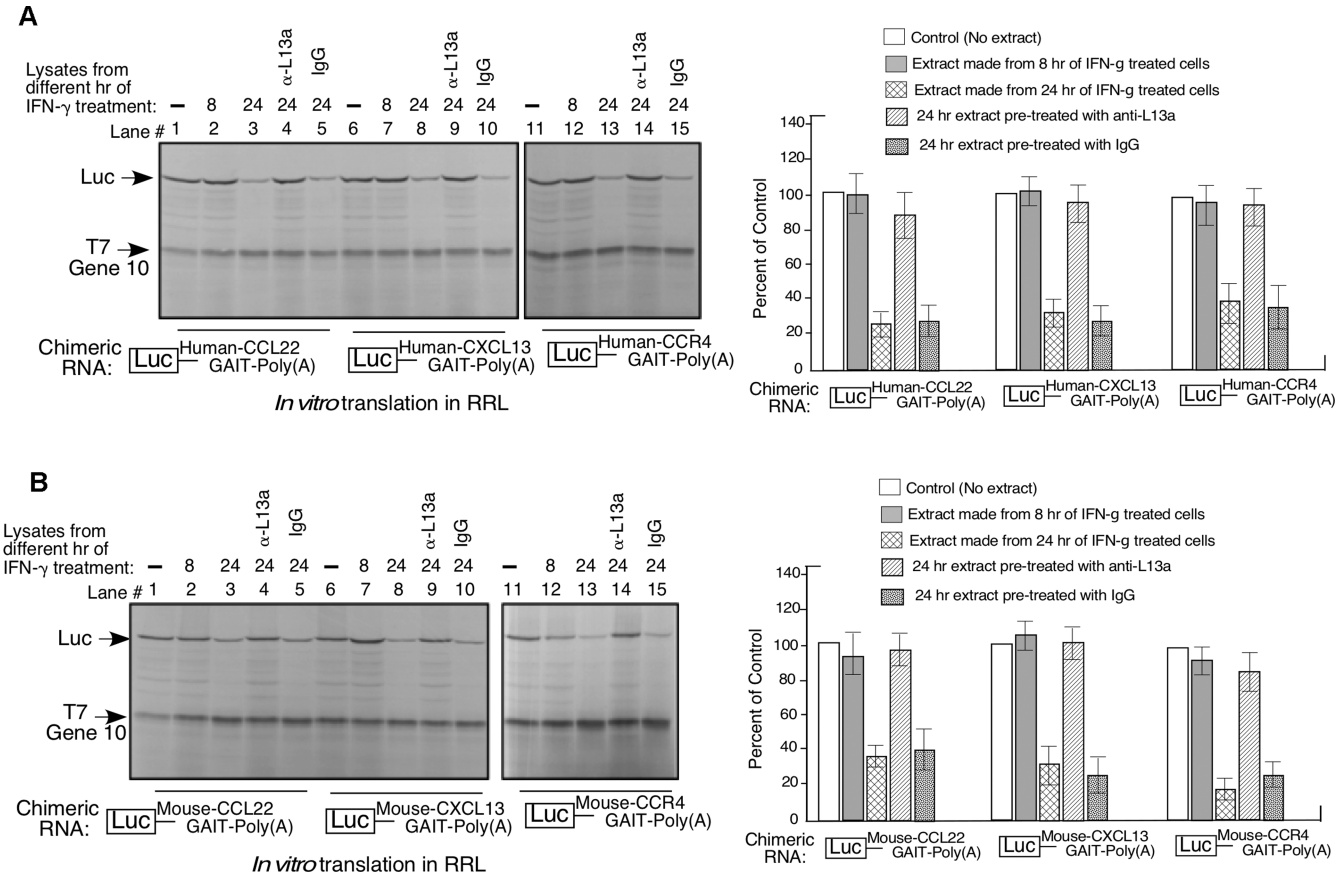

Figure 5. Both human and murine CCL22, CXCL13 and CCR4 GAIT elements direct L13a-dependent translational silencing in IFN-γ activated human monocytes. Luciferase reporter mRNAs harboring human (A) and murine (B) CCL22, CXCL13 or CCR4 GAIT elements in their 3′UTRS were translated *in vitro* in rabbit reticulocyte lysates (in the presence of [^{35}S]-Methionine). Extracts prepared from U937 cells treated for 8 or 24 h with IFN-γ were added to the translation reactions as indicated above each lane. α-L13a and IgG indicate pre-treatment of extracts with antibodies. [^{35}S]-Methionine-labeled luciferase and T7 gene 10 cRNA (included in each reaction as a specificity control) translation products were separated by SDS-PAGE (indicated by arrows). Each figure is the representative of an experiment performed in triplicate. The bar diagrams in the right panel of both (**A**) and (**B**) show quantifications of the results presented in the gel. Ratio of the band intensities of the newly translated [^{35}S]-labeled luciferase protein and T7 gene 10 protein (as internal control) were determined using NIH image 64 software. Each bar diagram is the representative of an experiment performed in triplicate. The quantifications with standard deviations were shown. Percent inhibition was determined by comparing with the control lane with no extract.

that the so-called WHEP domain of the core GAIT complex component glutamyl-prolyl tRNA synthetase (EPRS) directs binding of the complex to the GAIT element-bearing mRNAs; however, simultaneous presence of all four GAIT complex proteins (EPRS, GAPDH, NSAP1 and phospho-L13a) in human cells is necessary to substantiate high affinity binding (26). Absence of NSAP1 from the murine system suggests that it is not likely to play a key role. On the side of the RNA element, it is remarkable that different GAIT elements are predicted to have very similar secondary structures/folds (albeit of different stabilities), despite their differences in nucleotide sequence (Figure 1). It is possible, however, that differences in the nucleotide composition of different GAIT elements may lead to differences in affinity towards the GAIT–protein complex. As a first step toward answering this question, we performed additional RNA EMSA analyses using human Cp, CCL22, CXCL13 and CCR4 GAIT elements with different amounts of human U937 monocyte cell extract in order to determine apparent affinities of GAIT RNA–protein binding. Cell extracts were prepared from U937 cells treated for 24 h with IFN-γ, a condition known to lead to active GAIT complex formation (6,8), and were titrated into binding reactions over a 40-fold range (0.05–2.0 μg/reaction). EMSA bands corresponding to GAIT-bound and unbound GAIT RNA element probes were quantified. The fraction of bound RNA was plotted as a function of the apparent GAIT-complex concentration in the extract (estimated as described in Methods) in order to derive the apparent equilibrium binding constant (K_d), which is a measure of the affinity between the RNA-binding protein complex and its target element. This method revealed that all four analyzed GAIT elements had different affinities towards the GAIT complex. The Cp GAIT element showed the highest affinity ($K_d = 4.5 \times 10^{-13}$ M and the CXCL13 GAIT element had the lowest affinity ($K_d = 2.7 \times 10^{-12}$ M), thus revealing a range in affinities for the four tested GAIT elements of ∼20-fold (Figure 7).

To further examine the relative binding affinities of the different GAIT elements, we tested their ability to compete with each other for GAIT complex binding in EMSA experiments. Thus, unlabeled CCL22, CXCL13 and CCR4 GAIT element probes were titrated (up to 100-fold excess com-

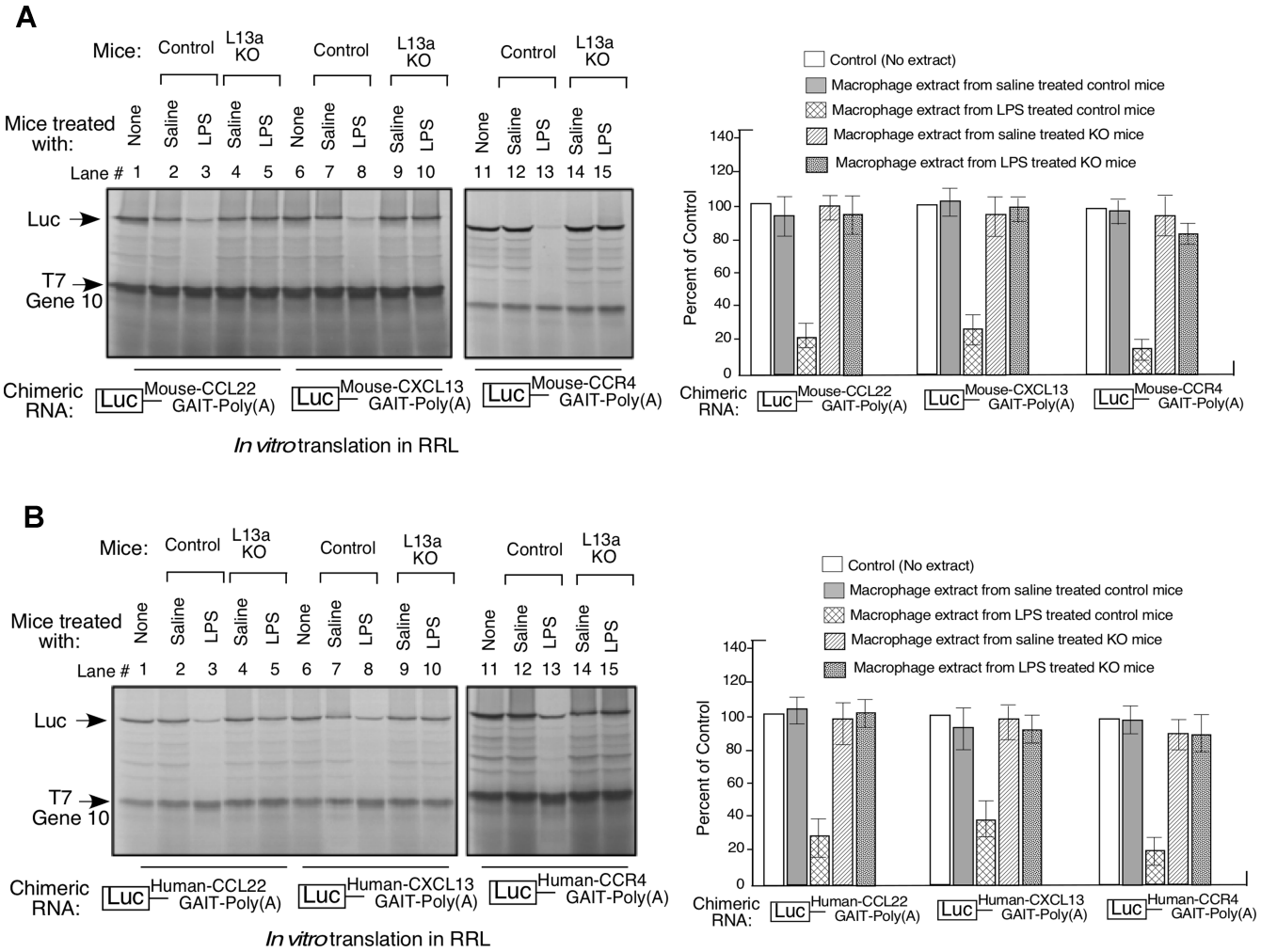

Figure 6. Both human and murine CCL22, CXCL13 and CCR4 GAIT elements direct L13a-dependent translational silencing in murine macrophages isolated from LPS treated mice. Luciferase reporter mRNAs harboring murine (**A**) and human (**B**) CCL22, CXCL13 or CCR4 GAIT elements in their 3′UTRS were used. *In vitro* translation reactions were performed as described for Figure 5 except the extracts were prepared from peritoneal macrophages of saline- and LPS-treated control and macrophage-specific L13a KO mice; Each figure is the representative of an experiment performed in triplicate. The bar diagrams in the right panel of both (A) and (B) show quantifications of the results presented in the gel as described in the figure legend of Figure 5.

pared to labeled probe) into binding reactions containing 2 μg/reaction of extract prepared from U937 cells treated with IFN-γ for 24 h and labeled human Cp GAIT element probe. Quantification of the bound Cp element fraction allowed determination of the equilibrium dissociation constant for each competitor (K_c). This showed that while the unlabeled Cp GAIT element can efficiently outcompete the labeled probe from 'homologous' Cp element-GAIT protein complexes (4×10^{-13} M), heterologous (non-Cp) unlabeled GAIT elements were less effective in disrupting Cp element-GAIT protein complexes (Figure 8). Based on K_c, the affinities of CCL22, CXCL13 and CCR4 elements for GAIT protein binding were all ∼20-fold lower than the affinity of the Cp element (Figure 8). The obtained K_d and K_c data are consistent with each other, and together demonstrate that different GAIT elements have different affinities for the GAIT complex. Notably, these differences in affinity do not show any correlation with the thermodynamic stability of the stem–loop structures formed by the GAIT elements (indicated by predicted ΔG values shown in Figure 1). All images presented in Figures 7 and 8 are the representatives of experiments performed in triplicate and the standard deviations were shown in the graphs on the right.

Different segments within the overall conserved GAIT element structure contribute to differential GAIT RNA–protein binding affinity

The different affinities of the four GAIT elements under study towards GAIT protein complex suggest that sequence-unrelated, but structurally conserved GAIT elements may form different sets of contacts with proteins of the GAIT complex. To gain further insight into the molecular basis of these differences, we performed toeprinting analysis. This technique uses primer extension to examine interactions between RNA sequences and RNA-binding proteins (analogous to fingerprinting analysis of DNA–protein binding) and is capable of determining the specific nucleotide positions occupied by proteins as well as the relative affinity of binding at each position (23,27,28). The

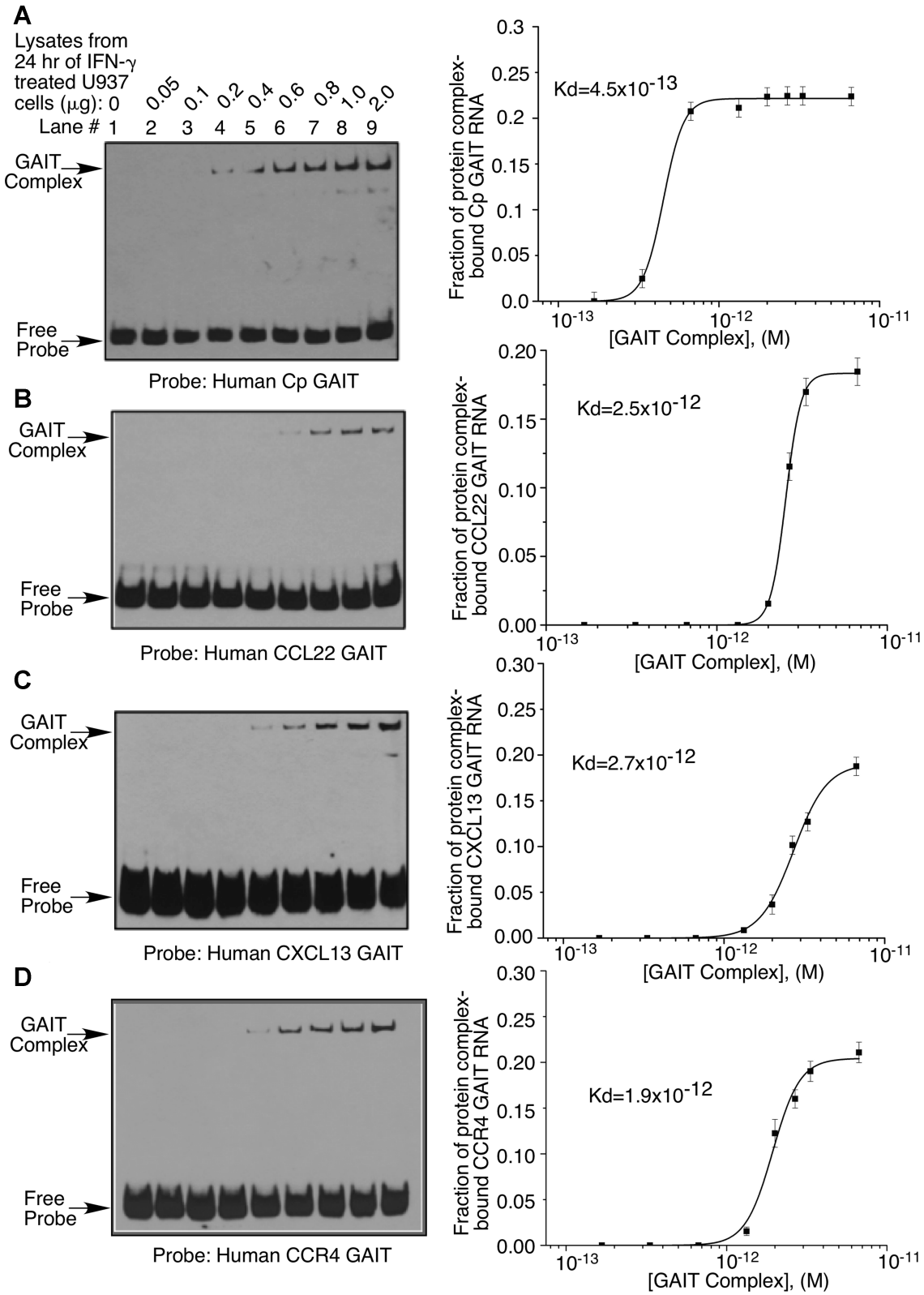

Figure 7. Measurement of GAIT RNA–protein complex equilibrium dissociation constants by RNA-EMSA for (**A**) Cp, (**B**) CCL22, (**C**) CXCL13 and (**D**) CCR4 GAIT elements. Left panels: EMSA using the indicated GAIT RNA element probes (15 fmol 5′ end-labeled) and different amount of extract prepared from U937 cells treated with IFN-γ for 24 h. Right panel: The fraction of bound RNA is plotted as a function of the GAIT concentration. A fit to the Hill equation is shown and the *K*d for each particular experiment is given. Each figure is the representative of an experiment performed in triplicate. The standard deviations have been presented in the graphs on the right.

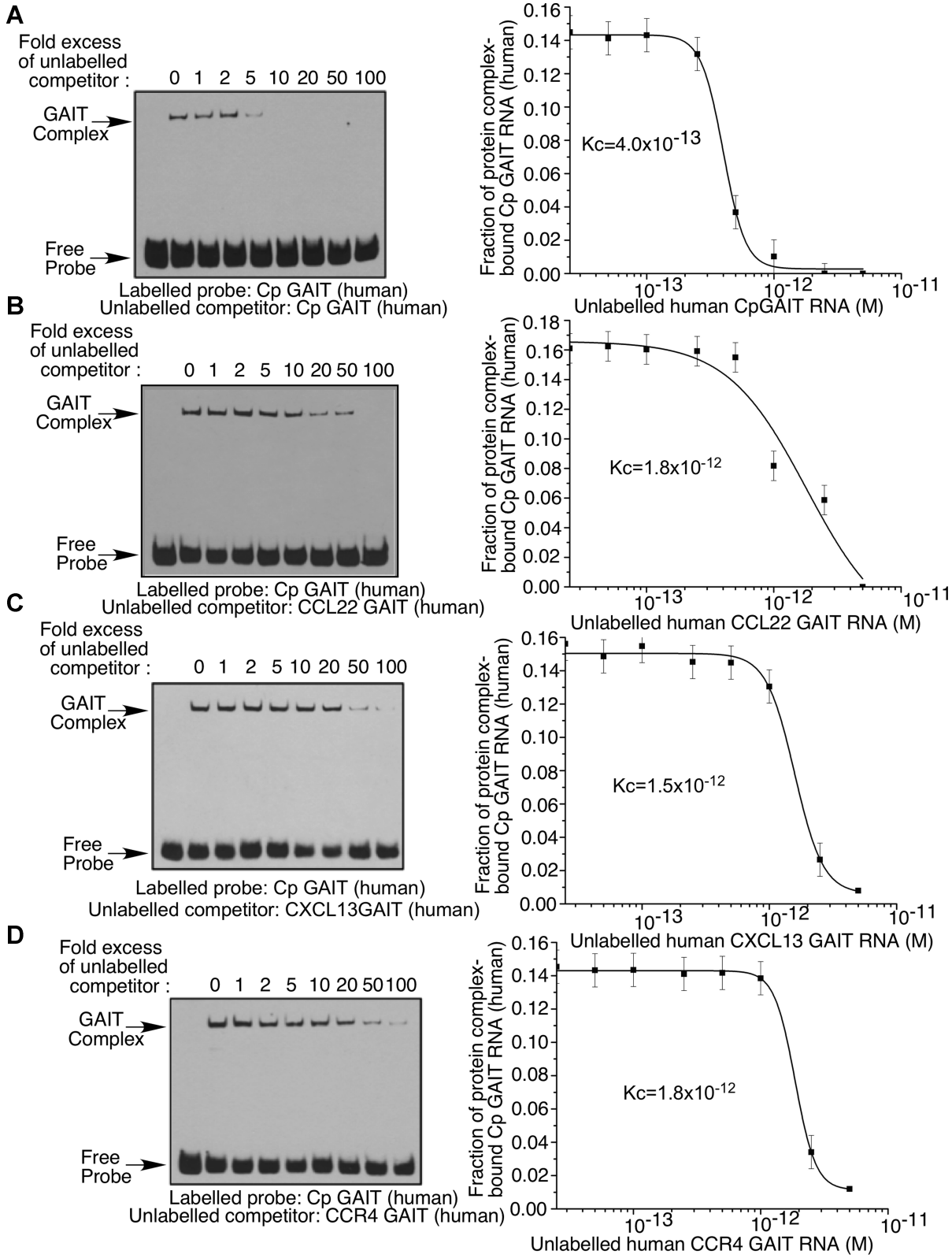

Figure 8. Competition mobility shift experiments. Titration of unlabeled GAIT RNA element probes from (**A**) Cp, (**B**) CCL22, (**C**) CXCL13 and (**D**) CCR4 into Cp GAIT element binding reactions. Left panels: RNA EMSA using U937 cell extracts prepared from 24 h of IFN-γ treated cell and the indicated labeled and unlabeled probes. Right panel: The fraction of bound Cp GAIT element probe in shifted complexes was quantified by and plotted against competitor RNA concentration. The equilibrium dissociation constant of the competitor (K_c) is shown. Each figure is the representative of an experiment performed in triplicate. The standard deviations have been presented in the graphs on the right.

strength of primer extension stops (indicated by band intensity) is generally correlated with the affinity of protein binding at that particular position in the RNA. Strong and weak stops observed for Cp, CCL22, CXCL13 and CCR4 GAIT element RNAs incubated with extracts from IFN-γ-treated U937 cells are indicated in Figure 9 by red and black arrows, respectively. All of these stops are only or predominantly observed in the presence of GAIT protein complex present in the extract obtained from IFN-γ treated cells. These predominant stops were not observed upon incubation of the probes with extracts made from untreated cells (Supplementary Figure S3) or only probe without any extracts (Figure 9, right most lanes). Equal intensities of the full-length products of 110 nucleotides were also observed in all four samples, however the regions were not shown. These results show that the GAIT protein complex forms a substantially different set of contacts on each of the tested GAIT elements. The total number of contacts, their positions and their relative strengths all differ between elements. For example, the high affinity (Figures 7 and 8) Cp GAIT element forms 5 strong protein contacts located in the internal bulge and the proximal helical stem of the RNA. The lower affinity CCL22, CXCL13 and CCR4 GAIT elements all have fewer strong contacts than the Cp element (ranging from 0 in CCR4 to 4 in CXCL13), but more relatively weak contacts (Figure 9). The location of both strong and weaker contacts varies between the four tested elements (Figure 9). The data do not identify particular nucleotides or particular parts of the stem–loop structure that are universally important for GAIT RNA–protein binding. Thus, while these findings provide a molecular basis for the observed differences in affinities of the heterogeneous GAIT elements for the RNA-binding GAIT protein complex, the precise GAIT element features required for strong vs weak GAIT RNA–protein binding remain to be determined.

DISCUSSION

Chemokines and chemokine receptors are the critical arm of inflammatory response that mobilizes the immune cells at the site of inflammation and infection (29,30). Resolution of inflammation relies on production of pro-resolving molecules as well as activation of intracellular pathways leading to ordered silencing of pro-inflammatory molecules (1–5). Silencing of a diverse set of pro-inflammatory chemokines and chemokine receptors in macrophages and monocytes is directed by heterogeneous GAIT elements located in the 3′UTRs of their mRNAs. Inflammatory stimuli initially result in enhanced expression of these pro-inflammatory proteins, but also induce formation of the GAIT protein complex, which binds to the RNA elements and blocks translation, thus creating a negative feedback loop. The physiological importance of this system was demonstrated in our prior studies with macrophage-specific L13a KO mice, which showed that L13a-dependent and GAIT element mediated translational silencing plays a critical role in the resolution of inflammation and in the pathogenesis of several inflammation-associated diseases (13–15).

Here, we report structural insights and functional analysis of a subset of newly identified inflammation-associated GAIT elements, those found in mRNAs. Remarkably, there is no apparent sequence homology among these CCL22, CXCL13 and CCR4 elements or the canonical Cp GAIT element. In contrast we found that they can all adopt very similar stem–loop structures as predicted by *in silico* modeling (Figure 1) and confirmed by 2D and 1D-^{1}H NMR analysis (Figure 2 and Supplementary Figure S1). The defined elements all form specific complexes with the RNA-binding GAIT protein complex (Figures 3 and 4) and direct translational silencing of reporter mRNAs *in vitro* when inserted into their 3′UTRs (Figures 5 and 6). Both of these activities were shown to be L13a-dependent. However, despite their similar structures and functions, we found that affinities of the CCL22, CXCL13 and CCR4 GAIT elements towards GAIT protein complex differ substantially (by an order of magnitude) in comparison with the canonical Cp GAIT element (Figures 7 and 8). These differences in affinity might be due to specific variations in the overall conserved GAIT element stem–loop secondary structure shown in Figure 1, such as differences in the size and RNA sequence composition of the bulge and hairpin loops. Our toeprinting data (Figure 9 and Supplementary Figure S3) provides physical evidence of differences in the number and strength of specific contacts formed between the GAIT protein complex and different GAIT RNA elements. These differences likely define the relative affinities of the elements for the GAIT complex.

Although only four GAIT elements were analyzed in the current work, our data suggest the existence of at least two different classes of GAIT elements defined by their affinity for GAIT protein complex binding. This would include a high affinity class represented by the Cp GAIT element and a lower affinity class represented by elements such as those found in the CCL22, CXCL13 and CCR4 mRNAs. Although Cp is currently the only known member of the high affinity group, it is possible that other members will be identified.

It is notable that GAIT-mediated translational silencing relies on the conserved structure of target RNA elements rather than any conserved sequence motifs. For most other RNA–protein interactions with physiological outcomes, conserved sequences in the RNAs direct protein binding and subsequent downstream effects. Examples of this include the control of iron metabolism through IRE element-dependent regulation of ferritin and transferrin receptor synthesis (31), tuning of the REDOX system by SECIS element-dependent translational control of the selenoproteins (32), DICE element-mediated translational control in erythroid differentiation (33,34) and shaping of anterior-posterior patterning in Drosophila embryos by TCE element-dependent translational control of the nanos mRNA (35). Why the GAIT system, which represents a critical defense mechanism against uncontrolled inflammation, relies on structural homology rather than sequence conservation remains unclear. However, our finding that structure-directed binding of the GAIT protein complex to GAIT RNA elements of different sequences is non-uniform (involving different binding affinities) suggests that the system may allow for more than ‘all-or-none’ control. It can be speculated that indiscriminate binding of the GAIT complex to all GAIT elements harbored in target mRNAs with equal affinity could compromise desirable spatial and tem-

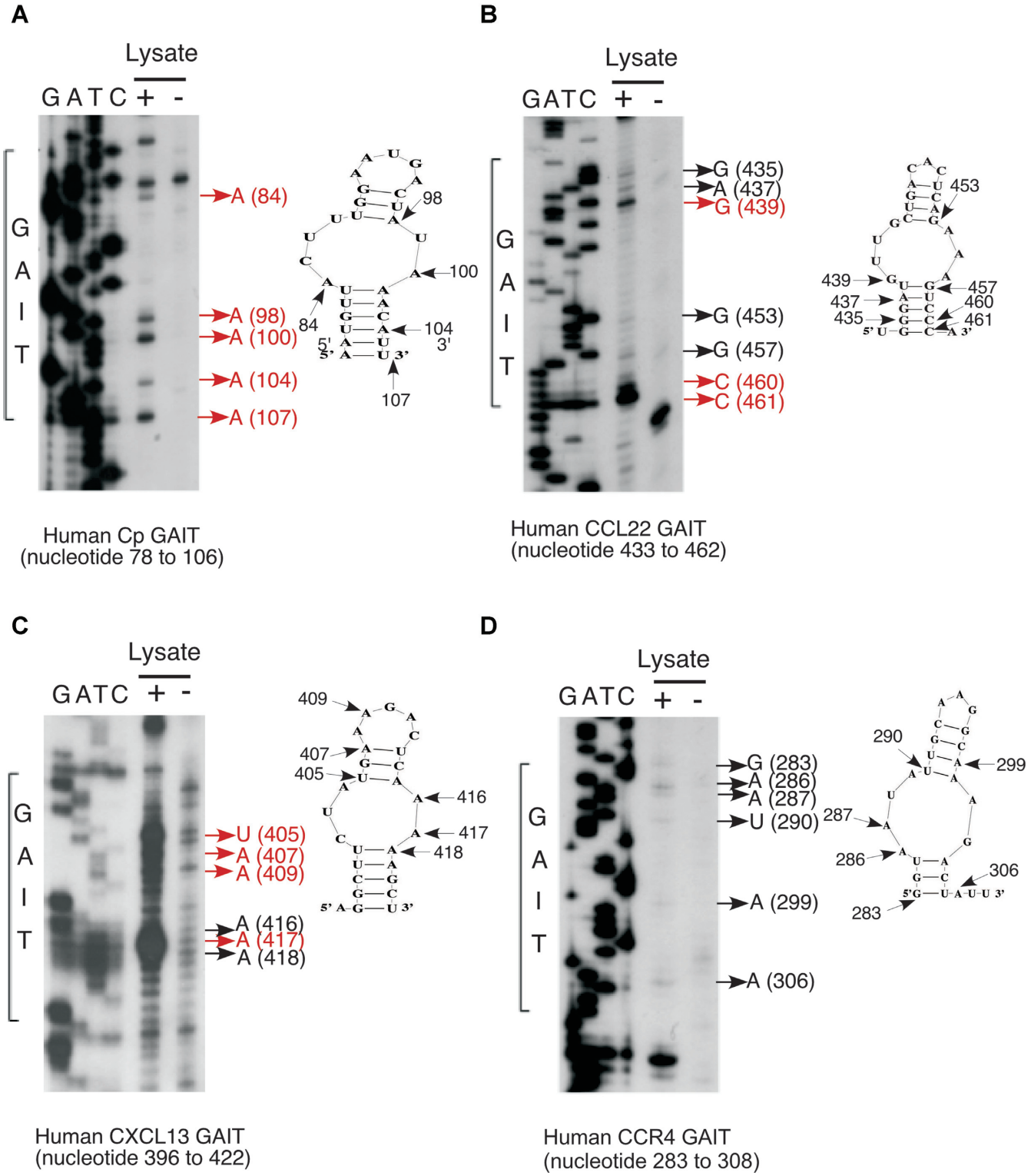

Figure 9. Toeprinting analysis of GAIT RNA–protein complex formation. GAIT element-containing RNA fragments derived from the 3′ UTRs of human Cp (**A**), CCL22 (**B**), CXCL13 (**C**) and CCR4 (**D**) mRNAs were incubated in the presence or absence of protein extracts prepared from U937 cells that were treated with IFN-γ for 24 h. Reactions were analyzed by primer extension analysis and separated on denaturing polyacrylamide gels. The gels were dried and bands were visualized by autoradiography. Red arrows indicate strong primer extension stops; black arrows indicate weaker stops. Results from the experiment using untreated cells were shown in Supplementary Figure S3.

poral expression of the targets in the microenvironment of inflammation. Thus, the heterogeneity of GAIT element sequences and resulting differences in GAIT protein binding contacts and affinities may provide a system for fine-tuning the resolution of inflammation.

AVAILABILITY

'Foldalign' is an open source platform (http://foldalign.ku.dk). 'RNAstructure' is an open source platform (http://rna.urmc.rochester.edu/RNAstructure.html).

SUPPLEMENTARY DATA

Supplementary Data are available at NAR Online.

ACKNOWLEDGEMENTS

Author contributions: B.S.T., A.A.K. and B.M. conceived and designed the study. A.B. and N.J. performed most of the experiments. A.B., N.J., B.S.T., A.A.K. and B.M. conducted analyses and interpreted results. B.M., A.B., B.S.T. and A.A.K. wrote the manuscript, and all authors contributed to the final version of the manuscript.

FUNDING

National Institute of Health (NIH) [HL79164 to B.M., HL121779 to A.A.K., GM101979 to B.S.T]; Cleveland State University Office of Research and the Center for Gene Regulation in Health and Disease (GRHD). Funding for open access charge: NIH [HL79164]; Center for Gene Regulation in Health and Disease (GRHD) of Cleveland State University.
Conflict of interest statement. None declared.

REFERENCES

1. Anderson,P. (2010) Post-transcriptional regulons coordinate the initiation and resolution of inflammation. *Nat. Rev. Immunol.*, **10**, 24–35.
2. Mazumder,B., Li,X. and Barik,S. (2010) Translation control: a multifaceted regulator of inflammatory response. *J. Immunol.*, **184**, 3311–3319.
3. Carpenter,S., Ricci,E.P., Mercier,B.C., Moore,M.J. and Fitzgerald,K.A. (2014) Post-transcriptional regulation of gene expression in innate immunity. *Nat. Rev. Immunol.*, **14**, 361–376.
4. Kafasla,P., Skliris,A. and Kontoyiannis,D.L. (2014) Post-transcriptional coordination of immunological responses by RNA-binding proteins. *Nat. Immunol.*, **15**, 492–502.
5. Piccirillo,C.A., Bjur,E., Topisirovic,I., Sonenberg,N. and Larsson,O. (2014) Translational control of immune responses: from transcripts to translatomes. *Nat. Immunol.*, **15**, 503–511.
6. Mazumder,B. and Fox,P.L. (1999) Delayed translational silencing of ceruloplasmin transcript in gamma interferon-activated U937 monocytic cells: role of the 3′ untranslated region. *Mol. Cell Biol.*, **19**, 6898–6905.
7. Mazumder,B., Seshadri,V., Imataka,H., Sonenberg,N. and Fox,P.L. (2001) Translational silencing of ceruloplasmin requires the essential elements of mRNA circularization: poly(A) tail, poly(A)-binding protein, and eukaryotic translation initiation factor 4G. *Mol. Cell Biol.*, **21**, 6440–6449.
8. Mazumder,B., Sampath,P., Seshadri,V., Maitra,R.K., Dicorleto,P.E. and Fox,P.L. (2003) Regulated release of L13a from the 60S ribosomal subunit as a mechanism of transcript-specific translational control. *Cell*, **115**, 187–198.
9. Sampath,P., Mazumder,B., Seshadri,V., Gerber,C.A., Chavatte,L., Kinter,M., Ting,S.M., Dignam,J.D., Kim,S., Driscoll,D.M *et al.* (2004) Noncanonical function of glutamyl-prolyl-tRNA synthetase: gene-specific silencing of translation. *Cell*, **119**, 195–208.
10. Sampath,P., Mazumder,B., Seshadri,V. and Fox,P.L. (2003) Transcript-selective translational silencing by gamma interferon is directed by a novel structural element in the ceruloplasmin mRNA 3′ untranslated region. *Mol. Cell Biol.*, **23**, 1509–1519.
11. Kapasi,P., Chaudhuri,S., Vyas,K., Baus,D., Komar,A.A., Fox,P.L., Merrick,W.C. and Mazumder,B. (2007) L13a blocks 48S assembly: role of a general initiation factor in mRNA-specific translational control. *Mol. Cell*, **25**, 113–126.
12. Vyas,K., Chaudhuri,S., Leaman,D.W., Komar,A.A., Musiyenko,A., Barik,S. and Mazumder,B. (2009) Genome-wide polysome profiling reveals an inflammation-responsive posttranscriptional operon in gamma interferon-activated monocytes. *Mol. Cell Biol.*, **29**, 458–470.
13. Poddar,D., Basu,A., Baldwin,W.M. 3rd, Kondratov,R.V., Barik,S. and Mazumder,B. (2013) An extraribosomal function of ribosomal protein L13a in macrophages resolves inflammation. *J. Immunol.*, **190**, 3600–3612.
14. Basu,A., Poddar,D., Robinet,P., Smith,J.D., Febbraio,M., Baldwin,W.M. 3rd and Mazumder,B. (2014) Ribosomal protein L13a deficiency in macrophages promotes atherosclerosis by limiting translation control-dependent retardation of inflammation. *Arterioscler. Thromb. Vasc. Biol.*, **34**, 533–542.
15. Poddar,D., Kaur,R., Baldwin,W.M. 3rd and Mazumder,B. (2016) L13a-dependent translational control in macrophages limits the pathogenesis of colitis. *Cell Mol. Immunol.*, **13**, 816–827.
16. Smyth,R.P., Despons,L., Huili,G., Bernacchi,S., Hijnen,M., Mak,J., Jossinet,F., Weixi,L., Paillart,J.C., von Kleist,M. *et al.* (2015) Mutational interference mapping experiment (MIME) for studying RNA structure and function. *Nat. Methods*, **12**, 866–872.
17. Havgaard,J.H., Lyngso,R.B., Stormo,G.D. and Gorodkin,J. (2015) Pairwise local structural alignment of RNA sequences with sequence similarity less than 40%. *Bioinformatics*, **21**, 1815–1824.
18. Havgaard,J.H., Torarinsson,E. and Gorodkin,J. (2007) Fast pairwise structural RNA alignments by pruning of the dynamical programming matrix. *PLoS Comput. Biol.*, **3**, 1896–1908.
19. Torarinsson,E., Havgaard,J.H. and Gorodkin,J. (2007) Multiple structural alignment and clustering of RNA sequences. *Bioinformatics*, **23**, 926–932.
20. Delaglio,F., Grzesiek,S., Vuister,G.W., Zhu,G., Pfeifer,J and Bax,A. (1995) NMRpipe: a multidimensional spectral processing system based on UNIX pipes. *J. Biomol. NMR*, **6**, 277–293.
21. Johnson,B.A. and Blevins,R.A. (1994) NMR View: A computer program for the visualization and analysis of NMR data. *J. Biomol. NMR*, **4**, 603–614.
22. Ryder,S.P., Recht,M.I. and Williamson,J.R. (2008) Quantitative analysis of protein-RNA interactions by gel mobility shift. *Methods Mol. Biol.*, **488**, 99–115.
23. Malmgren,C., Engdahl,H.M., Romby,P. and Wagner,E.G. (1996) An antisense/target RNA duplex or a strong intramolecular RNA structure 5′ of a translation initiation signal blocks ribosome binding: the case of plasmid R1. *RNA*, **2**, 1022–1032.
24. Mestas,J. and Hughes,C.C. (2004) Of mice and not men: differences between mouse and human immunology. *J. Immunol.*, **172**, 2731–2738.
25. Arif,A., Chatterjee,P., Moodt,R.A. and Fox,P.L. (2012) Heterotrimeric GAIT complex drives transcript-selective translation inhibition in murine macrophages. *Mol. Cell. Biol.*, **32**, 5046–5055.
26. Jia,J., Arif,A., Ray,P.S. and Fox,P.L. (2008) WHEP domains direct noncanonical function of glutamyl-Prolyl tRNA synthetase in translational control of gene expression. *Mol. Cell*, **29**, 679–690.
27. Pisareva,V.P., Pisarev,A.V., Komar,A.A., Hellen,C.U. and Pestova,T.V. (2008) Translation initiation on mammalian mRNAs with structured 5′UTRs requires DExH-box protein DHX29. *Cell*, **135**, 1237–1250.
28. Pisarev,A.V., Unbehaun,A., Hellen,C.U. and Pestova,T.V. (2007) Assembly and analysis of eukaryotic translation initiation complexes. *Methods Enzymol.*, **430**, 147–177.
29. Charo,I.F. and Ransohoff,R.M. (2006) The many roles of chemokines and chemokine receptors in inflammation. *N. Engl. J. Med.*, **354**, 610–621.

30. Shi,C. and Pamer,E.G. (2011) Monocyte recruitment during infection and inflammation. *Nat. Rev. Immunol.*, **11**, 762–774.
31. Muckenthaler,M.U., Galy,B. and Hentze,M.W. (2008) Systemic iron homeostasis and the iron-responsive element/iron-regulatory protein (IRE/IRP) regulatory network. *Annu. Rev. Nutr.*, **28**, 197–213.
32. Krol,A. (2002) Evolutionarily different RNA motifs and RNA–protein complexes to achieve selenoprotein synthesis. *Biochimie*, **84**, 765–774.
33. Ostareck,D.H., Ostareck-Lederer,A., Wilm,M., Thiele,B.J., Mann,M. and Hentze,M.W. (1997) mRNA silencing in erythroid differentiation: hnRNP K and hnRNP E1 regulate 15-lipoxygenase translation from the 3′ end. *Cell*, **89**, 597–606.
34. Ostareck,D.H., Ostareck-Lederer,A., Shatsky,I.N. and Hentze,M.W. (2001) Lipoxygenase mRNA silencing in erythroid differentiation: The 3′UTR regulatory complex controls 60S ribosomal subunit joining. *Cell*, **104**, 281–290.
35. Crucs,S., Chatterjee,S. and Gavis,E.R. (2000) Overlapping but distinct RNA elements control repression and activation of nanos translation. *Mol. Cell*, **5**, 457–467.